TOWARDS HIGHLY EFFICIENT THERMOELECTRICS: $Ca_3Co_4O_{9+\delta} \cdot n\ CaZrO_3$ COMPOSITE

[#]ONDŘEJ JANKOVSKÝ*, ŠTĚPÁN HUBER*, **, DAVID SEDMIDUBSKÝ*, LADISLAV NÁDHERNÝ*, TOMÁŠ HLÁSEK*, ZDENĚK SOFER*

*Institute of Chemical Technology Prague, Technicka 5, Prague, Czech Republic
**Institute of Physics, ASCR, v.v.i., Cukrovarnicka 10, Prague, Czech Republic

[#]E-mail: Ondrej.Jankovsky@vscht.cz

Submitted April 11, 2014; accepted July 4, 2014

Keywords: Misfit cobaltites, Thermoelectric materials, Composites

We successfully prepared $Ca_3Co_4O_{9+\delta} \cdot n\ CaZrO_3$ composites by a ceramic route. These composites were characterized by X-Ray diffraction, differential thermal analysis, thermogravimetric analysis and scanning electron microscopy. Moreover, transport properties (Seebeck coefficient, electrical resistivity and thermal conductivity) were measured and the thermoelectric figure of merit ZT was determined. Addition of $CaZrO_3$ led to a suppression of thermal conductivity of the samples. A high thermal stability connected to the interesting thermoelectric properties made this material a potential candidate for the p type cell in the high-temperature thermoelectric batteries.

INTRODUCTION

High power consumption as well as the need for green energy makes thermoelectric energy recovery one of the possible energy sources for the future. Apart from of the high thermal stability, suitable thermoelectric material should in particular exhibit high Seebeck coefficient, low electrical resistivity and low thermal conductivity. Fulfilling all these conditions simultaneously is a challenging issue since these parameters are strongly interrelated.

Misfit layered cobaltites ($Ca_3Co_4O_{9+\delta}$, $Bi_{2-x}Sr_2Co_{1.85}O_{7+\delta}$, etc.) are the promising candidates for high-temperature applications. [1-3] To reach higher figure of merit it is essential to optimize microstructure and also the chemical composition. Microstructure can be modified by applying different methods of thermal treatment, by particles size control, formation pressures [4] as well as by addition of various dopants.

Addition of dopants can lead to a formation of single phase material, where dopants (usually metal cations) are incorporated into the structure. Synthesis of $Ca_{3-x}A_xCo_{4-y}B_yO_{9+\delta}$, where A is Nd [5], Lu [6], Dy [7], Ga [8], Gd [9], Y [10] and B is Ti [11], leading to higher figure of merit have been reported. Also two-phase materials (composites) can be formed by dopants addition. For instance, $Ca_{3-x}Bi_xCo_4O_{9+\delta} \cdot z$ Ag system has been synthetized, [12] where Ag precipitated as a second phase on grain boundaries. Addition of Ag increased the densification and texture development of the composite. Fabrication of materials containig phase mixtures $Ca_3Co_4O_{9+\delta} \cdot Ca_3Co_2O_6$ or $Bi_{2-x}Sr_2Co_{1.85}O_{7+\delta} \cdot A$, where A is $Bi_2Sr_2CoO_6$, $Sr_6Co_5O_{15}$, $Bi_{24}Co_2O_{39}$ or Co_3O_4 [13-16], can significantly influence thermoelectric properties.

In this paper, we are going to present a different approach. We prepared $Ca_3Co_4O_{9+\delta} \cdot n\ CaZrO_3$ (n = 0; 0.1; 0.2 and 0.5) composites by ceramic route. The main idea of this experiment is to suppress the thermal conductivity due to the scattering of the phonons on the grains of $CaZrO_3$ leading to higher figure of merit.

EXPERIMENTAL

Samples with compositions $Ca_3Co_4O_{9+\delta}$ (CC-Zr0), $Ca_3Co_4O_{9+\delta} \cdot 0.1\,CaZrO_3$ (CC-Zr1), $Ca_3Co_4O_{9+\delta} \cdot 0.2\,CaZrO_3$ (CC-Zr2) and $Ca_3Co_4O_{9+\delta} \cdot 0.5\ CaZrO_3$ (CC-Zr3) were prepared by a solid state reaction. Starting powders of $CaCO_3$, Co_2O_3 and $CaZrO_3$ were homogenized in agate mortar. After the homogenization powders were calcined in the platinum crucible at 1123 K for 24 h. Then the samples were re-homogenized and calcined at 1173 K for the next 24 h. The next step of the synthesis was the milling in the epicyclic mill Retsch PM 100 for 40 min.

After the milling, powders were uniaxially pressed (500 MPa, 1 min) and sintered in oxygen atmosphere at 1213 K for 100 h.

The phase composition of the samples was evaluated from powder X-Ray Diffraction (XRD) patterns recorded within the range 2θ = 5 – 80° on X'Pert PRO diffractometer in Bragg-Brentano parafocusing geometry using CuK_α radiation.

The samples density was determined by weighting the pellets and measuring their volume. Due to the porous nature of the prepared samples the accurate pycnometric measurements could not be performed.

Differential thermal analysis (DTA) and thermogravimetric analysis (TG) were performed simultaneously from 293 K to 1373 K on Setaram STA Setsys Evolution with a heating rate 10 $K \cdot min^{-1}$ in a dynamic air atmosphere.

The material morphology was investigated using scanning electron microscopy (SEM) with a FEG electron source (Tescan Lyra dual beam microscope).

Transport properties (electrical resistivity, thermal conductivity and Seebeck coefficient) were measured using four-probe method (self-designed equipment). The measurement was carried out in a vacuum cell integrated into a closed-cycle helium cryostat.

The high temperature thermal conductivity was calculated from the thermal diffusivity, which was measured by laser flash analysis (LFA) on Linseis LFA 1000 apparatus with an Nd-YAG Laser from ambient temperature to 573 K. The tests were performed in vacuum, which precludes the measurements at higher temperatures due to significant change of oxygen stoichiometry of $Ca_3Co_4O_{9+\delta}$. Therefore, values of thermal conductivity were extrapolated to higher temperatures. The heat capacity of $Ca_3Co_4O_{9+\delta}$ necessary for the conversion of diffusivity to thermal conductivity was taken from our previous study. [3]

The figure of merit *ZT* representing the coefficient of thermoelectric efficiency was calculated using the following equation:

$$ZT = T \cdot \frac{S^2}{\rho \cdot \lambda} \qquad (1)$$

where T is thermodynamic temperature, S is Seebeck coefficient, ρ is electrical resistivity and λ is thermal conductivity.

RESULTS AND DISCUSSION

The composites $Ca_3Co_4O_{9+\delta}$ · 0.1 $CaZrO_3$ (CC-Zr1), $Ca_3Co_4O_{9+\delta}$ · 0.2 $CaZrO_3$ (CC-Zr2) and $Ca_3Co_4O_{9+\delta}$ · 0.5 $CaZrO_3$ (CC-Zr3) were successfully prepared. Moreover, the undoped sample $Ca_3Co_4O_{9+\delta}$ (CC) was prepared as a reference (see the structure in Figure 1). The prepared materials were analyzed by XRD, TDA, TG and SEM and their *ZT* was calculated from the Seebeck coefficient, electrical resistivity and thermal conductivity.

First the phase composition of prepared composites was determined by XRD. The XRD patterns showed that samples CC-Zr1, CC-Zr2 and CC-Zr3 contained two phases, $Ca_3Co_4O_{9+\delta}$ [17] and $CaZrO_3$ [18]. The reference sample CC was single-phase containing only the layered cobaltite, $Ca_3Co_4O_{9+\delta}$ (Figure 2). All samples had a density 3.69 g/cm^3, which corresponded to 77 % of the maximum theoretical density of $Ca_3Co_4O_{9+\delta}$. Such results indicated that addition of $CaZrO_3$ had no influence on the overall density.

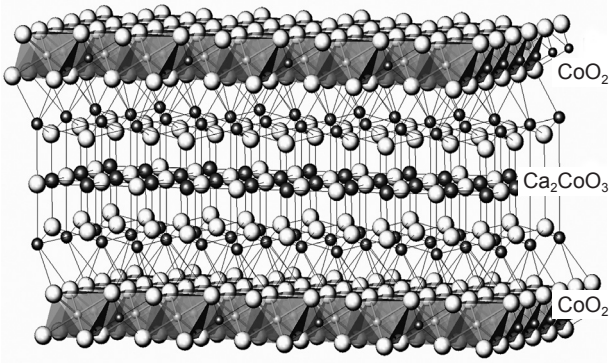

Figure 1. Structure of misfit layered cobaltite $Ca_3Co_4O_{9+\delta}$.

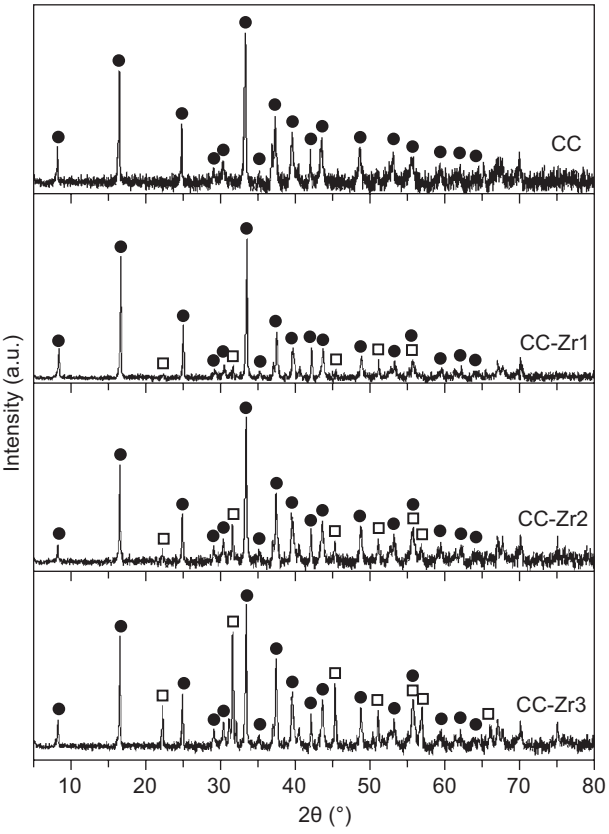

Figure 2. Powder XRD patterns of CC, CC-Zr1, CC-Zr2 and CC-Zr3. The symbols ● indicate the presence of $Ca_3Co_4O_{9+\delta}$ [17] and the symbols □ stand for $CaZrO_3$ [18]

DTA and TG were used to probe the thermal stability of CC-Zr3, which contained the highest amount of $CaZrO_3$. (Figure 3) Similar thermal behavior can be expected for other samples. The first small effect at 1173 K was accompanied by a weight loss and it is apparently associated with crossing the narrow miscibility region of the $Ca_3Co_{3.93\pm x}O_{9+\delta}$ phase and precipitation of $Ca_3Co_2O_6$ phase with lower oxygen content, as recently shown by Sedmidubský et al. [17]. The second peak at 1222 K corresponds to peritectoid decomposition of $Ca_3Co_4O_{9+\delta}$ into $Ca_3Co_2O_6$ and $Co_{1-x}Ca_xO$. The last peak at 1326 K can be clearly attributed to the decomposition of $Ca_3Co_2O_6$ to $Co_{1-x}Ca_xO$ and $Ca_{1-x}Co_xO$ revealing a large miscibility gap. The second phase comprised in the composite, $CaZrO_3$, obviously behaves as an inert additive from the point of view of thermal stability, Moreover, the results of thermal analysis show that this composite can be used in a wide temperature range up to 1170 K, which is sufficient for use in high-temperature thermoelectric batteries.

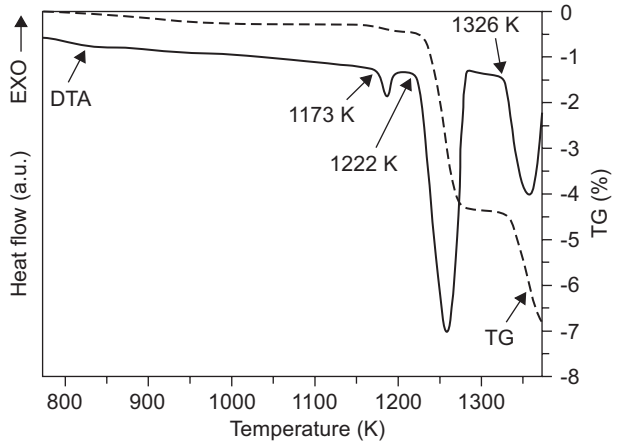

Figure 3. DTA and TG analysis of CC-Zr-3 in air atmosphere.

The microstructure was analyzed by SEM (Figure 4). The laminar grains of $Ca_3Co_4O_{9+\delta}$ are darker, while the smaller and brighter grains correspond to $CaZrO_3$. It is obvious that even the long-term milling of the precursor was not sufficient to achieve ideal homogenous distribution of $CaZrO_3$ in the composite. Moreover, $CaZrO_3$ partially formed agglomerates.

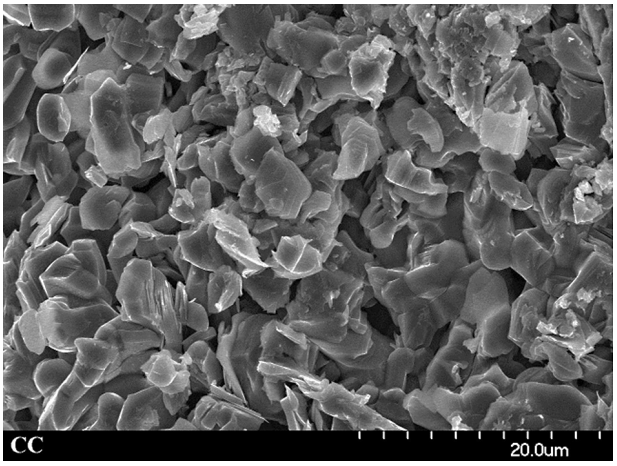

a) CC

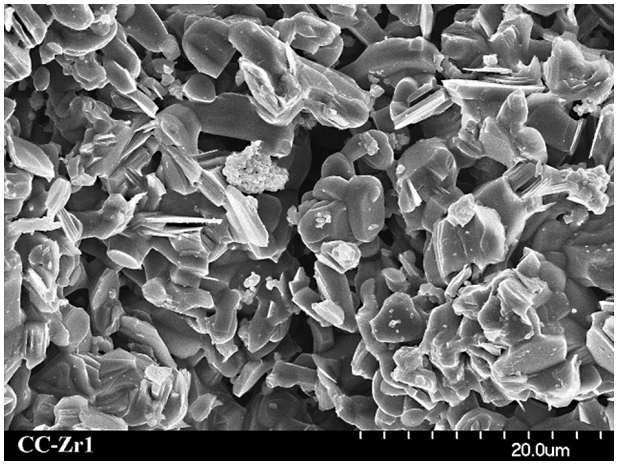

b) CC-Zr1

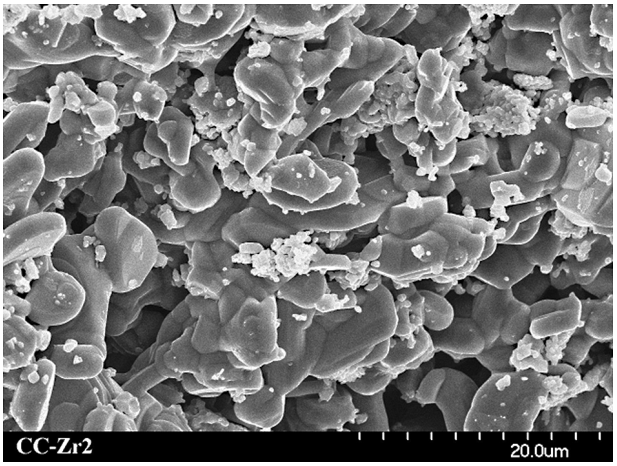

c) CC-Zr2

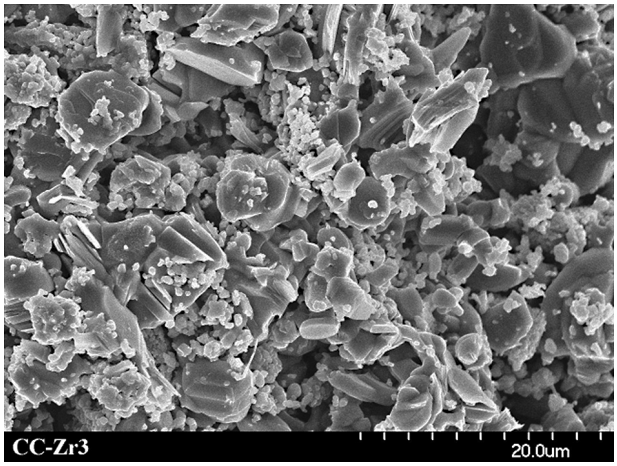

d) CC-Zr3

Figure 4. SEM images of a) CC, b) CC-Zr1, c) CC-Zr2 and d) CC-Zr3 composites (fractures).

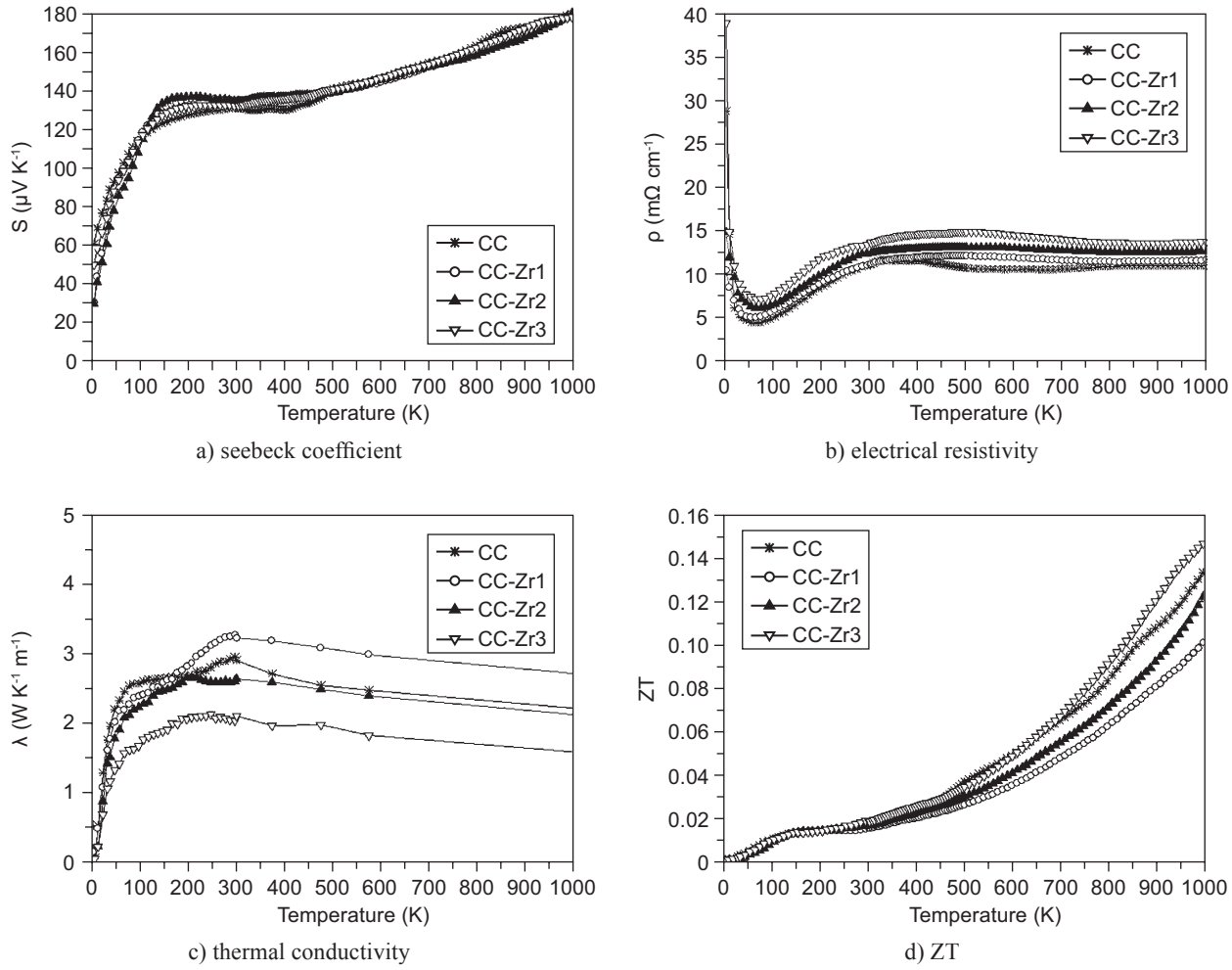

Figure 5. a) Seebeck coefficient, b) thermal conductivity, c) electrical resistivity and d) ZT of CC, CC-Zr1, CC-Zr2 and CC-Zr3 composites.

In the next step, the transport properties were measured (Figure 5). Addition of $CaZrO_3$ had no influence on the Seebeck coefficient whose value reached $S \sim 180\ \mu V \cdot K^{-1}$ for all samples at 1000 K. On the other hand, the addition of $CaZrO_3$ had an appreciable influence on the thermal conductivity: higher amount significantly reduced thermal conductivity (CC-Zr3) if compared to CC. The reason why this effect appeared only in the case of CC-Zr3 can be explained in terms of relatively low density (high porosity) of the samples. Small particles of $CaZrO_3$ were simply located on much larger grains of $Ca_3Co_4O_{9+\delta}$ and they did not form 'bridges' or 'necks'. Also the formation of $CaZrO_3$ agglomerates reduced the effectiveness of the doping. Higher amount of $CaZrO_3$ also increased the electrical resistivity, but not so dramatically as was the effect on thermal conductivity.

The figure of merit of the prepared composites is shown in lower right panel of Figure 5. In order to evaluate its temperature dependence up to highest temperatures, it was necessary to extrapolate the thermal conductivity above 600 K from the values obtained by LFA. The assumption of decreasing behavior of thermal conductivity above the room temperature is logical: at higher temperatures most phonon modes are excited and common collisions between phonons occur. This phonon-phonon scattering is responsible for the decrease of thermal conductivity. Sample CC-Zr3 achieved higher ZT than CC at 1000 K; however, the increase was not as significant as we expected. The problem is that thermal conductivity and electrical resistivity are strongly intercorrelated and the decrease of thermal conductivity can cause a simultaneous increase of the electrical resistivity. However, a different scattering mechanism for electrons and phonons is anticipated due to a different wave length and group velocity so the electron transport is believed to be less affected by the impurity phase.

CONCLUSION

We prepared and characterized three $Ca_3Co_4O_{9+\delta}$· *n* $CaZrO_3$ composites and compared their transport properties to the pure $Ca_3Co_4O_{9+\delta}$. The measurements confirmed the hypothesis that the addition of $CaZrO_3$

decreased the thermal conductivity, whereas the values of Seebeck coefficient and electrical resistivity did not change a lot. This leads to the elevation of the figure of merit especially at high temperatures for the most doped sample CC-Zr3. Higher pressures or other compaction procedures such as SPS or HP will be necessary to efficiently apply lower amounts of $CaZrO_3$ with similar results. Such procedures can lead to highly dense composites with outstanding thermoelectric properties.

Acknowledgement

This work was supported by Czech Science Foundation (Project No. 13-17538S).

REFERENCES

1. Hejtmánek J., Knížek K., Maryško M., Jirák Z., Sedmidubský D., Jankovský O., Huber Š., Masschelein P., Lenoir B.: J. Appl. Phys. *111*, 07D715 (2012).
2. Jankovský O., Sedmidubský D., Rubešová K., Sofer Z., Leitner J., Ružička K., Svoboda P.: Thermochim. Acta *582*, 40 (2014).
3. O. Jankovský D. S., Z. Sofer, P. Simek, J. Hejtmanek: Ceram.Sil. *56*, 139 (2012).
4. Kenfaui D., Chateigner D., Gomina M., Noudem J. G.: J. Alloys Comp. *490*, 472 (2010).
5. Prevel M., Reddy E. S., Perez O., Kobayashi W., Terasaki I., Goupil C., Noudem J. G.: Japanese Journal of Applied Physics, Part 1: Regular Papers and Short Notes and Review Papers *46*, 6533 (2007).
6. Tang G. D., Wang Z. H., Xu X. N., Qiu L., Xing L., Du Y. W.: J. Mater. Sci. *45*, 3969 (2010).
7. Wang D., Chen L., Wang Q., Li J.: J. Alloys Compd. *376*, 58 (2004).
8. Nong N. V., Liu C. J., Ohtaki M.: J. Alloys Compd. *491*, 53 (2010).
9. Tang G. D., Tang C. P., Xu X. N., He Y., Qiu L., Lv L. Y., Wang Z. H., Du Y. W.: J. Electron. Mater. *40*, 504 (2011).
10. Liu H. Q., Song Y., Zhang S. N., Zhao X. B., Wang F. P.: J. Phys. Chem. Solids *70*, 600 (2009).
11. Xu L., Li F., Wang Y.: J. Alloys Compd. *501*, 115 (2010).
12. Song Y., Sun Q., Zhao L., Wang F., Jiang Z.: Mater. Chem. Phys. *113*, 645 (2009).
13. Jankovský O., Sedmidubský D., Sofer Z., Rubešová K., Růžička K., Svoboda P.: J. Eur. Ceram. Soc. *34*, 1219 (2014).
14. Jankovský O., Sedmidubský D., Sofer Z., Leitner J., Růžička K., Svoboda P.: Thermochim. Acta *575*, 167 (2014).
15. Jankovský O., Sedmidubský D., Sofer Z.: J. Eur. Ceram. Soc. *33*, 2699 (2013).
16. O. Jankovsky D. S., Z. Sofer, J. Capek, K. Ruzicka: Ceram. Sil. *57*, 83 (2013).
17. Sedmidubský D., Jakeš V., Jankovský O., Leitner J., Sofer Z., Hejtmánek J.: J. Solid State Chem. *194*, 199 (2012).
18. Levin I., Amos T. G., Bell S. M., Farber L., Vanderah T. A., Roth R. S., Toby B. H.: J. Solid State Chem. *175*, 170 (2003).